Talanta 285 (2025) 127375

Contents lists available at ScienceDirect

Talanta

journal homepage: www.elsevier.com/locate/talanta

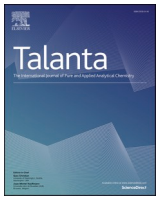

Development of molecularly imprinted polymer-based electrochemical sensors for the detection of UV filters in aquatic ecosystems

Chiara Sarti [a,b,*], Lea Falcon [b], Alessandra Cincinelli [a,c], Tania Martellini [a], Iva Chianella [b]

[a] Department of Chemistry "Ugo Schiff", University of Florence, Via della Lastruccia 3, 50019, Sesto Fiorentino, Italy
[b] Surface Engineering and Precision Centre, Faculty of Engineering and Applied Sciences, Cranfield University, MK43 0AL, Bedford, United Kingdom
[c] Consorzio Interuniversitario Nazionale per le Scienze Ambientali (CINSA) unità locale Università degli Studi di Firenze, Via della Lastruccia, 3-13, 50019, Sesto Fiorentino, Italy

ARTICLE INFO

Keywords:
Benzophenone-3 (BP-3)
Octocrylene (OC)
Molecularly imprinted polymers (MIPs)
Electrochemical sensors
Electrochemical impedance spectroscopy (EIS)
Wastewater monitoring

ABSTRACT

The presence of organic UV filters (OUVAs) has been detected worldwide in aquatic ecosystems. These pollutants, originating from various anthropogenic sources, can persist and transform within wastewater treatment plants (WWTPs), posing a potential environmental hazard. In this framework, this research presents electrochemical sensors based on molecularly imprinted polymers (MIPs) for the selective detection of Benzophenone-3 (BP-3) and Octocrylene (OC), two of the OUVA most spread in the aquatic environment, to overcome the analytical challenges related to the quantification of this class of contaminants in wastewater samples. Key parameters, including the selection of the electropolymerization conditions, the template washing, polymer surface blocking, and analyte re-binding conditions, were optimized to maximize the selectivity and sensitivity. Electrochemical detection was performed using electrochemical impedance spectroscopy (EIS) supported by an electrochemical probe. In addition, cross-reactivity tests were carried out in the presence of possible interferents, selected based on their size, chemical structure, and occurrence in wastewater samples. The sensors demonstrated significant selectivity and sensitivity for the target analytes, with detection limits of 30 nM for BP-3 and 1 nM for OC, while tests on complex wastewater samples showed recovery rates of 77 % and 101 % for BP-3 and OC, respectively. The study yielded interesting results that could lead to a specific, cost-effective approach to enable widespread monitoring and support early detection of these increasingly relevant contaminants in wastewater samples.

1. Introduction

Contamination of aquatic ecosystems by organic UV filters (OUVAs) has become a major environmental concern in recent years. Among the most common OUVAs are benzophenone-3 (BP-3) and octocrylene (OC), which are widely used in sunscreen creams and other personal care products to protect against ultraviolet (UV) radiation [1]. Because of their extensive use, these chemicals are released into the environment through various pathways, including direct discharges from recreational activities into water bodies and as residuals from wastewater treatment plants (WWTPs) [2]. In fact, conventional WWTPs are not designed to effectively remove these emerging contaminants, resulting in their persistence in surface waters, and contributing to widespread pollution [3].

BP-3 and OC are known to have adverse effects on aquatic life. Studies have shown their potential to disrupt endocrine systems in marine organisms [4], cause coral bleaching [5], and even bioaccumulate in the food chain [6], posing long-term risks to both ecosystems and human health [7]. The increasing presence of these UV filters in the environment has therefore generated considerable scientific and regulatory interest, and the need for efficient monitoring and remediation strategies.

Traditional analytical techniques for the detection of BP-3 and OC, such as high-performance liquid chromatography (HPLC) and gas chromatography-mass spectrometry (GC-MS), are highly sensitive and accurate [8]. However, these methods have significant drawbacks, as they are costly and time-consuming, require sophisticated instrumentation and trained personnel. In addition, chromatographic techniques are often impractical for in-situ or large-scale monitoring, which is essential for comprehensive environmental assessments [9].

* Corresponding author. Department of Chemistry "Ugo Schiff", University of Florence, Via della Lastruccia 3, 50019, Sesto Fiorentino, Italy.
E-mail address: chiara.sarti@unifi.it (C. Sarti).

https://doi.org/10.1016/j.talanta.2024.127375
Received 29 October 2024; Received in revised form 27 November 2024; Accepted 10 December 2024
Available online 12 December 2024

In response to these limitations, the development of novel, cost-effective, and efficient detection methods has become a priority. Biosensors and affinity sensors, which are devices relying on a natural or artificial sensing element for the recognition of a target analyte, have great potential for in-situ diagnostics and large-scale monitoring [10]. Among all the available types of sensing elements, thanks to their robustness and stability, molecularly imprinted polymers (MIPs) are particularly suitable for in-field diagnostics [11]. MIPs are synthetic polymers designed to have highly selective binding sites for target molecules, due to a template-assisted polymerization, where the target analyte serves as a template during the polymer formation [12,13]. Functional monomers in a solution interact with the target analyte, forming a complex that is subsequently stabilized by polymerization. After the polymerization process, the template is removed, leaving behind molecular cavities within the polymer matrix. These cavities are selective recognition sites complementary in shape, size, and functional groups to the target compounds, enabling the MIP to specifically and selectively re-bind the analyte. The high degree of specificity, stability in harsh conditions, potential reusability, coupled with the transduction properties, make MIPs ideal receptors in sensing applications [14]. By incorporating these biomimetic ligands into electrochemical sensors, MIPs provide a robust platform for the sensitive and selective detection of several compounds. These characteristics, combined with the possibility of miniaturization and portability, make electrochemical MIP sensors particularly well-suited for environmental monitoring [11]. The development and optimization of these sensors could represent a significant step forward in addressing the challenges posed by emerging contaminants in aquatic ecosystems, providing a practical solution for their detection and, ultimately, their mitigation.

In this framework, the present study aims to develop and optimize electrochemical sensors based on MIPs for the detection of BP-3 and OC in aquatic environments. Electrochemical impedance spectroscopy (EIS) was selected here as the detection method, offering a sensitive, label-free technique to monitor the interaction between the MIP sensor and the target analytes. Despite the well-documented occurrence and potential toxicity of these compounds in aquatic ecosystems, to the best of our knowledge, this study is the first to develop affinity sensors designed for OUVA detection, with the ultimate goal of providing a specific and cost-effective approach that enables their widespread monitoring and early detection in water and wastewater samples.

2. Materials and methods

2.1. Chemicals

Phosphate-citrate buffer, ethanol (EtOH), methanol (MeOH), sulfuric acid (H_2SO_4), dimethyl sulfoxide (DMSO), sodium hydroxide (NaOH), salt potassium ferrocyanide ($Fe(CN)_6^{3-/4-}$), Triton X-100, and Tween 20 were from Sigma-Aldrich (Merck KGaA, Darmstadt, Germany). 2-Ethylhexyl 2-Cyano-3,3-diphenylacrylate (OC) was supplied by Lab Pro Inc (California, USA). Aniline and 2-Hydroxy-4-methoxybenzophenone (BP-3) were from Thermo Scientific (Thermo Fisher Scientific, Massachusetts, USA). DropSense screen-printed gold electrode 220AT and 220BT were supplied by Metrohm (Buckingham, UK).

2.2. Electrochemical impedance spectroscopy (EIS)

EIS was conducted using the Palmsens4 (Palmsens BV, Houten, Netherlands) to track changes at the electrode surface throughout all the sensor preparation steps, such as polymerization, washing, and blocking, as well as to evaluate analyte re-binding at varying concentrations. For the EIS measurements, 200 μL of 0.01 M $Fe(CN)_6^{3-/4-}$ in phosphate-citrate buffer (pH 5) was applied to the electrode and incubated for 15 min to reach equilibrium. After an additional equilibration period of 120 s, signals were recorded using a 0.01 a.c. and 0.12 d.c. voltage. The frequency ranged from 0.1 Hz to 50,000 Hz, with 6.5 data points per decade. Impedance results were represented as Nyquist plots and analyzed using an equivalent circuit model (shown in Supplementary Material, Fig. S1). The PSTrace 5.8' software (Palmsens BV, Houten, Netherlands) was used to fit the data and extract charge-transfer resistance (Rct) values.

2.3. Electrochemical polymerization of MIPs

Electrochemical polymerizations were conducted using a Palmsens4 potentiostat and screen-printed gold electrodes (SPGE), models 220BT (Metrohm DropSense S.L., Llanera, Spain), characterized by gold working and auxiliary electrodes, and silver reference electrode. A cleaning step was added before the polymerization, and this consisted of rinsing the electrodes with deionized water and performing 3 cyclic voltammetry (CV) scans from −0.6 V to +0.5 V at a scan rate of 0.05 V/s in the presence of 0.25 M H_2SO_4 (200 μL) on the electrode surface.

The electrochemical polymerization was performed by CV between −0.5 V and +0.8 V for 15 cycles at a scan rate of 0.05 V/s. For the BP-3 selective MIP layer, the polymerization was carried out with a solution constituted by 0.025 M aniline in H_2SO_4 0.25 M with 25 % EtOH, with a BP-3 concentration of 2.50 mM. A non-imprinted polymer (NIP), used as a control, was prepared following the same procedure but in the absence of BP-3.

For the OC selective MIP layer, the polymerization solution was constituted by 0.025 M aniline in H_2SO_4 0.25 M with 40 % EtOH, with OC concentration of 0.55 mM. The NIP control was prepared following the same procedure but in the absence of OC.

The schematic representation of the SPGE and the analytical protocol steps, starting from the MIP electropolymerization to the re-binding experiment, are summarized in Fig. 1.

2.4. Washing of template and electrode surface blocking

After the electropolymerization, all SPGE underwent a series of washing steps in an oven at 40 °C.

For BP-3 selective sensors, the electrodes were immersed in 4 different solutions, according to the following order: 75 % H_2SO_4 (0.1 M) + 25 % MeOH for 15 min, absolute MeOH for 5 min, 75 % NaOH (0.1 M) + 25 % MeOH for 15 min, and absolute MeOH for 5 min. This entire cycle was repeated twice. After washing, the electrode surface was blocked by incubating 200 μL of 0.01 % (v/v) Triton X-100 in phosphate-citrate buffer (0.025 M, pH 5) on the electrode for 1 h.

For OC selective sensors, the electrodes were immersed in 4 different solutions, according to the following order: 75 % H_2SO_4 (0.1 M) + 25 % DMSO for 15 min, absolute MeOH for 5 min, 75 % NaOH (0.1 M) + 25 % DMSO for 15 min, and absolute MeOH for 5 min. The entire cycle was repeated twice. After washing, the electrode surface was blocked by incubating 200 μL of 0.01 % (v/v) Tween 20 in phosphate-citrate buffer (0.025 M, pH 5) on the electrode for 1 h.

All the electrodes were then rinsed with deionized water and dried.

To ensure consistency in treatment and an accurate comparison of electrochemical responses, the NIP sensors underwent the same washing procedure as the respective MIPs.

2.5. Re-binding of analytes

BP-3 re-binding studies were performed with phosphate-citrate buffer (0.025 M, pH 5) initially in the absence (0 μM) and then with increasing concentrations of analyte (from 50 nM to 1 μM). Each solution was incubated on the SPGE for 60 min, washed with approximately 1 mL of Tween 20 0.01 % (v/v) in phosphate-citrate buffer (0.025 M, pH 5), and then rinsed with deionized water.

OC re-binding experiments were conducted using a phosphate-citrate buffer solution (0.025 M, pH 5) initially in absence (0 μM) and then at increasing concentrations of analyte (from 12.5 nM to 50 nM). Each solution was incubated on the electrode for 60 min, washed with

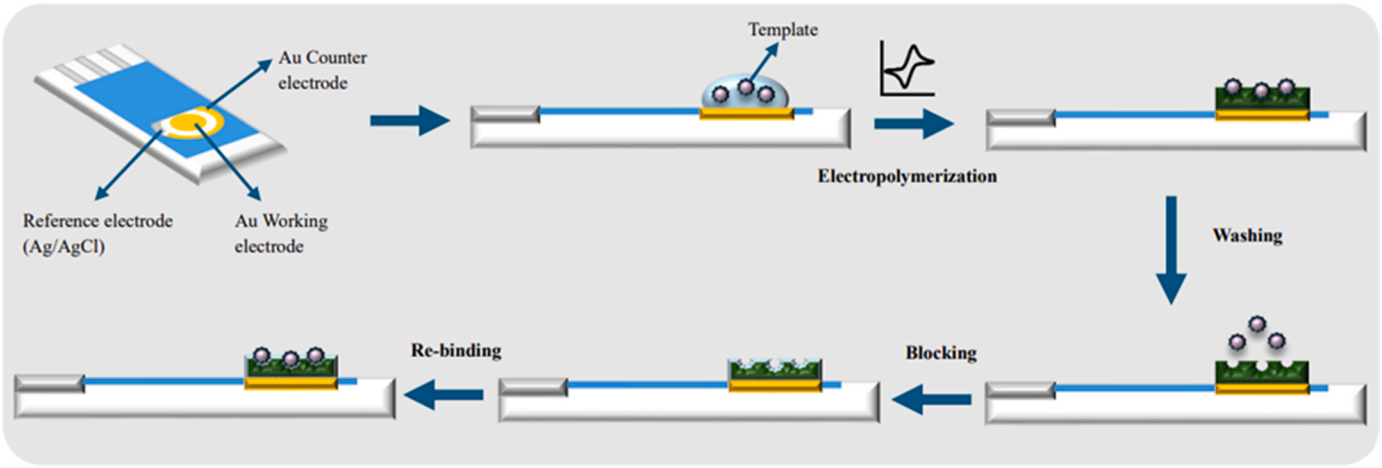

Fig. 1. Schematic representation of the gold screen-printed electrode (SPGE) and the analytical protocol steps: MIP electropolymerization, washing, blocking, and re-binding.

approximately 1 mL of Triton X-100 0.01 % (v/v) in phosphate-citrate buffer (0.025 M, pH 5), and then washed with deionized water.

EIS measurements and data fitting were performed after each analyte concentration test as described in section 2.2. The Rct values obtained for each concentration were normalized using the following equation:

$$\boldsymbol{Norm.\ Rct} = \frac{\boldsymbol{Rct_x} - \boldsymbol{Rct_0}}{\boldsymbol{Rct_0}}$$

where Rct_x is the charge-transfer resistance for a concentration X of analyte and Rct_0 is the charge-transfer resistance in the absence of analyte.

2.6. Selectivity and cross-reactivity studies

Selectivity experiments were conducted by comparing the Imprinting Factor (IF), calculated as the ratio of the signal obtained from the MIP to that from the NIP, for BP-3 and OC using both sensors, one optimized for BP-3 detection and the other for OC. Additionally, two potential interferents, ibuprofen and paracetamol, were selected based on their size, chemical structure, and widespread presence in water and wastewater, aligning with the main focus of this research. The structures of BP-3, OC and the investigated interfering molecules are reported in Fig. 2.

Re-binding tests were conducted using the procedure outlined in Section 2.5, with different solutions of each compound at a concentration of 0.1 μM incubated in parallel.

EIS measurements and data fitting were then performed for each compound test, as described in Section 2.2.

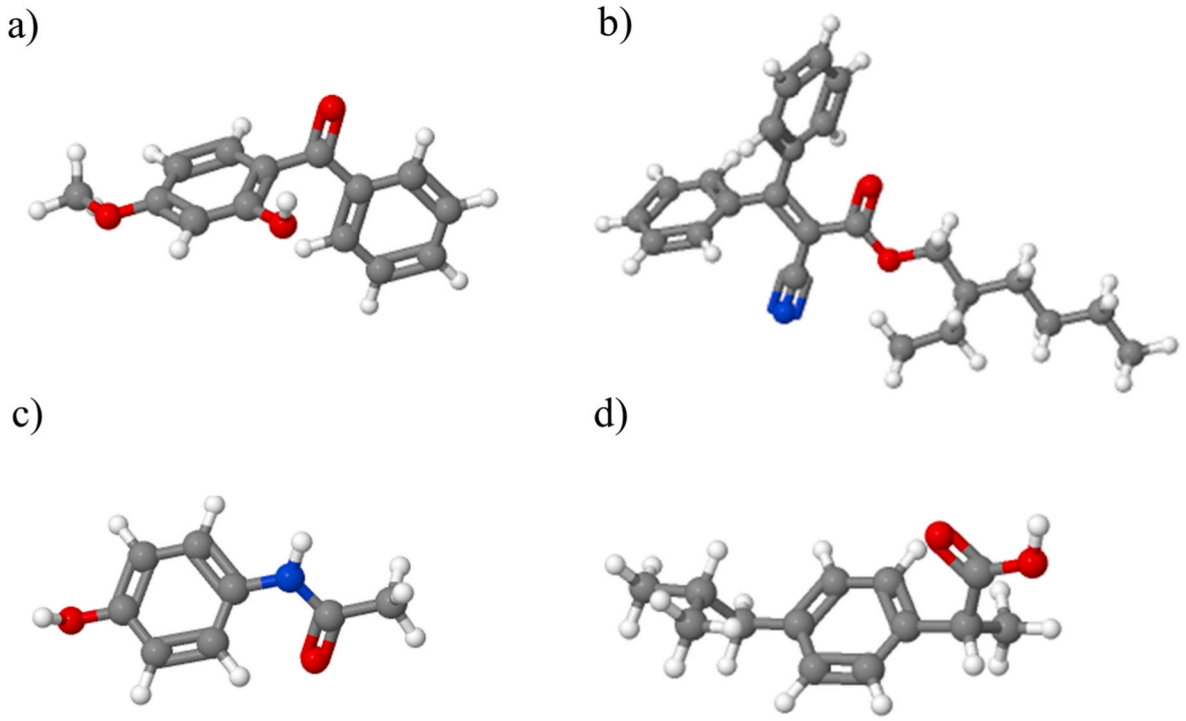

Fig. 2. Molecular structures of BP-3 (a), OC (b), paracetamol (c), and ibuprofen (d). Atoms are represented as follows: carbon (grey), hydrogen (white), oxygen (red), and nitrogen (blue).

2.7. Matrix effect and recovery test with wastewater samples

Water samples (1 L) were collected at the final effluent of the WWTP located at the UKCRIC National Research Facilities for Water and Wastewater Treatment at Cranfield University. After the collection, the sample was aliquoted into 50 mL Falcon tubes and stored at −20 °C until analysis. Given the complexity of the matrix, rich in organic matter and possible interferents, the matrix effect was evaluated by filtering the water samples through a 0.45 μm PTFE syringe filter (Corning Incorporated, New York, USA) and diluting 1:1 with phosphate-citrate buffer (pH 5). The samples were then spiked separately with increasing concentrations of BP-3 and OC (0.05, 0.1, and 0.5 μM and 0.0125, 0.05, and 0.25 μM for BP-3 and OC, respectively). A volume of 200 μL of the spiked sample was then applied to the electrodes and after 60 min of incubation and quick washing steps as explained in section 2.5 for the re-binding experiments, EIS measurements were performed as described in section 2.2.

To assess the recovery of analyte extraction, wastewater samples were instead first spiked with a known concentration of analyte (0.25 μM and 0.125 μM for BP-3 and OC, respectively). After spiking, the samples were filtered with a 0.45 μm syringe PTFE filter (Corning Incorporated, New York, USA), diluted 1:1 with phosphate-citrate buffer (pH 5) and placed on the electrode. EIS measurements were performed after 60 min of incubation and quick washing following the procedures described in section 2.2.

3. RESULTS and DISCUSSION

3.1. Optimization of MIP sensors

All steps of the analytical protocol were carefully optimized, from the electrochemical polymerization conditions to the re-binding process.

Given that the electropolymerization of polyaniline requires acidic conditions [15], one of the first parameters to optimize was the concentration of aniline and H_2SO_4 in the electropolymerization solution, as shown in Fig. 3. Initial tests were conducted in a solution of 50 mM H_2SO_4 with increasing concentrations of aniline: 2.5, 25, and 100 mM (Fig. 3a, b, c, respectively). Of the three, 25 mM aniline produced the best results (Fig. 3b), but the polymer film was still too thin. To address this limitation, the aniline concentration was kept constant at 25 mM, while the H_2SO_4 concentration was increased to 250 mM, resulting in a satisfactory increase of the polymer film (Fig. 3d). Additionally, the number of CV scans was also optimized to achieve a polymer layer with optimal thickness, striking a balance between maximizing the number of selective cavities in the MIP and minimizing non-specific interactions, both of which are proportional to the amount of polyaniline deposited. The results of such optimization, performed using OC as template, are shown in Fig. S2, reported in the Supplementary Material. The figure illustrates that when electropolymerization of aniline was conducted with 10 scans (polyaniline oxidation peaks at −0.1 V were approximately 10 μA for both MIP and NIP), negative Rct signals (lower resistance after incubation with OC) were observed, potentially indicative of a non-homogenous film with exposure of bare gold. In addition, there was no notable distinction between MIP and NIP signals, thereby not providing sufficient evidence to suggest the presence of imprinted cavities (Fig. S2a). Similarly, Fig. S2c illustrates that when electropolymerization of aniline was conducted with 20 scans (polyaniline oxidation peak height at −0.1 V for MIP and NIP exceeding 50 μA), the resulting polyaniline film was too challenging to block, likely due to the excessive thickness, as indicated by the elevated Rct signals obtained for the NIP sensors after OC re-binding. In contrast, when electropolymerization of polyaniline was conducted with 15 scans (polyaniline

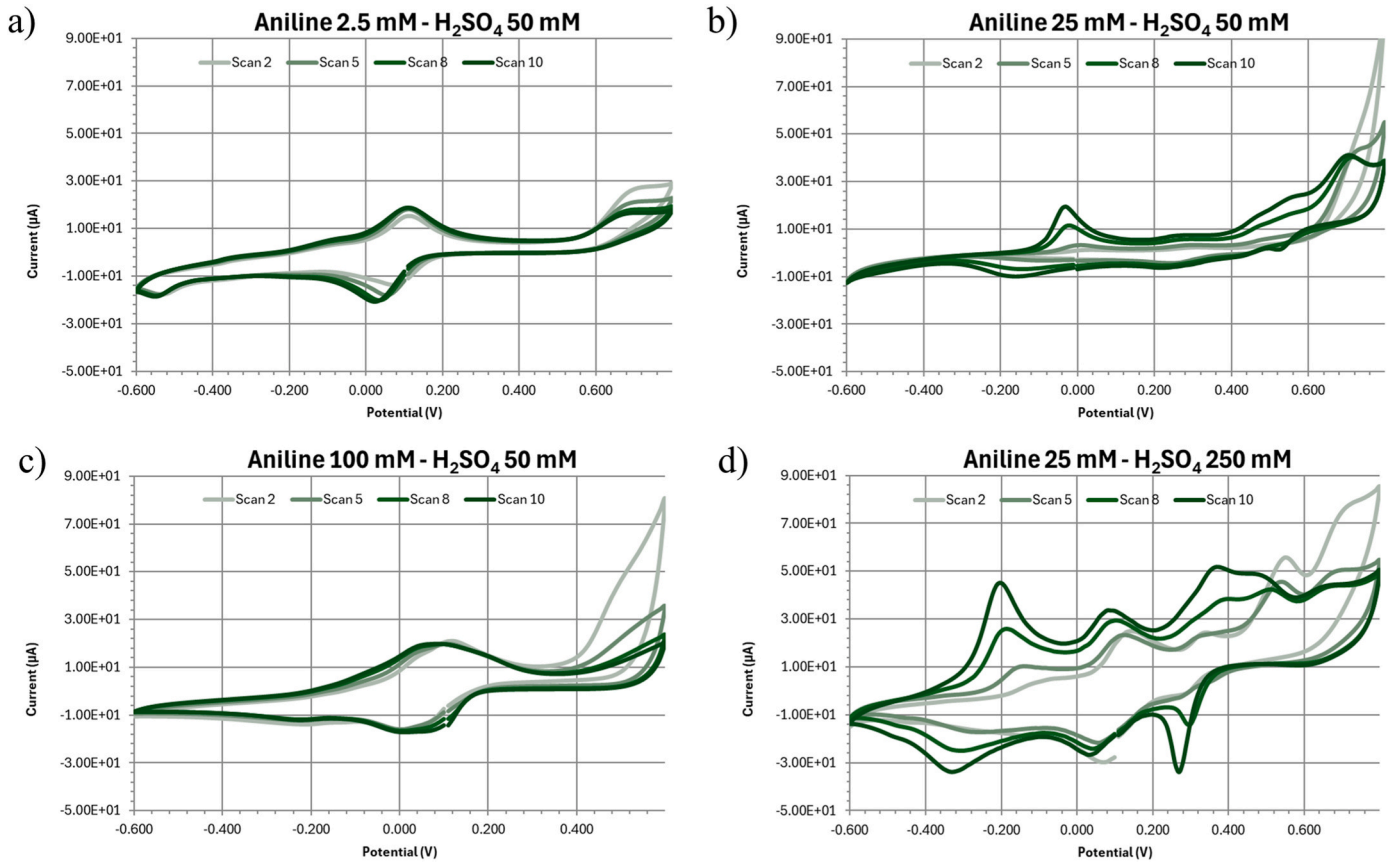

Fig. 3. Cyclic voltammetry (CV) after 2, 5, 8 and 10 scans with different concentrations of aniline and sulfuric acid in the electropolymerization solution: (a) aniline 2.5 mM in 50 mM H_2SO_4; (b) aniline 25 mM in 50 mM H_2SO_4; (c) aniline 100 mM in 50 mM H_2SO_4; (d) aniline 25 mM in 250 mM H_2SO_4 (d).

oxidation peak height at −0.1 V for MIP and NIP between 30 and 40 μA), the MIP and NIP layers appeared to have an appropriate thickness to demonstrate the presence of imprinted sites (increasing signals for MIP proportionally to the concentration of OC), without exhibiting the difficulty in blocking, as the binding of OC to the NIP was significantly lower than that to the MIP (Fig. S2 b). Similarly, the electropolymerization of BP-3 with 15 scans yielded polyaniline oxidation peaks (at −0.1 V) of approximately 30–40 μA, which generate layers with an optimal thickness for effective blocking and imprinting effect. Optimized CV of MIP and NIP layer for both analytes are shown in Fig. 4.

Optimizing the pH of the $Fe(CN)_6^{3-/4-}$ solution, used as an electrochemical probe for EIS analysis, was crucial to ensure suitable curves for subsequent fitting and data analysis, as well as to achieve stable and reproducible EIS measurements. Since aniline polymerization occurs under strongly acidic conditions (0.25 M H_2SO_4) and with the conductivity of polyaniline decreasing drastically at pH values higher than 6 [16], only various acidic pH values (between 1 and 5) were tested. As shown in Fig. S3, the best results (stable signals that could be easily fitted in an equivalent circuit) were obtained at pH 5, which was therefore chosen for all the EIS measurements.

Another key parameter to optimize was the concentration of templates added to the polymerization solution, aiming to balance the efficiency of polyaniline layer formation with the creation of an adequate number of selective cavities in the MIP. Indeed, insufficient binding sites results in insufficient specific interactions with the analyte, reducing the selectivity of the re-binding. However, the low solubility of OC in aqueous solutions posed a challenge in increasing its concentration in the polymerization solution, even when in presence of 25 % EtOH. Therefore, electropolymerization of MIP for OC was firstly performed with the maximum soluble concentration of 55 μM (template:monomer molar ratio of 1:450), which resulted in a lack of sufficient binding sites and hence a low specific affinity during the re-binding phase, as similar responses were obtained for MIP and NIP (Fig. 5a). To address this, the amount of EtOH in the polymerization solution was raised to 40 % (the maximum percentage demonstrating no interference with the polymerization of aniline), enabling to increase OC concentration to 0.55 mM (template:monomer ratio of 1:45) Although the template:monomer ratio was still low, enough binding cavities were obtained to demonstrate a specific MIP binding in subsequent analyte re-binding experiments, as shown in Fig. 5b.

For BP-3, the initial experiments were conducted using a template concentration of 2.50 mM, which was close to its maximum solubility in the chosen polymerization solution (0.025 M aniline in H_2SO_4 0.25 M with 25 % EtOH) and demonstrated specific binding to the MIP as compared to the NIP (Fig. S4). Such concentration also resulted in a molar ratio template:monomer of 1:10, which is often reported as optimal for electrochemical MIP synthesis [17,18].

Regarding the optimization of the sensor surface, various surfactants, including Triton X-100 and Tween 20, were tested as blocking agents to minimize non-specific interactions between the analytes and/or potential interferents and the polyaniline layer. Blocking efficiency was evaluated by measuring the response of MIP and NIP sensors after incubation with increasing concentrations of BP-3 and OC. As shown in Fig. 5c, for BP-3, effective blocking was achieved with Triton X-100, while Tween 20 resulted in a significant non-specific response. On the contrary, the best blocking performance for OC was obtained with Tween 20 (Fig. 5c), as Triton X seemed to affect the MIP sensor with binding of OC resulting in a negative Rct signal. In the attempt to optimize further the blocking for the OC sensor, a higher concentration of Tween 20 (0.05 %, (v/v) was also tested. As expected, the higher amount of surfactant generated lower signals both for MIP and NIP (Fig. 5d), but the IF values calculated as 1.8 and 2.1 for 0.05 % and 0.01 % of Tween 20 respectively, indicated that 0.01 % (v/v) was the optimal concentration and hence this was selected for all the OC MIP sensors.

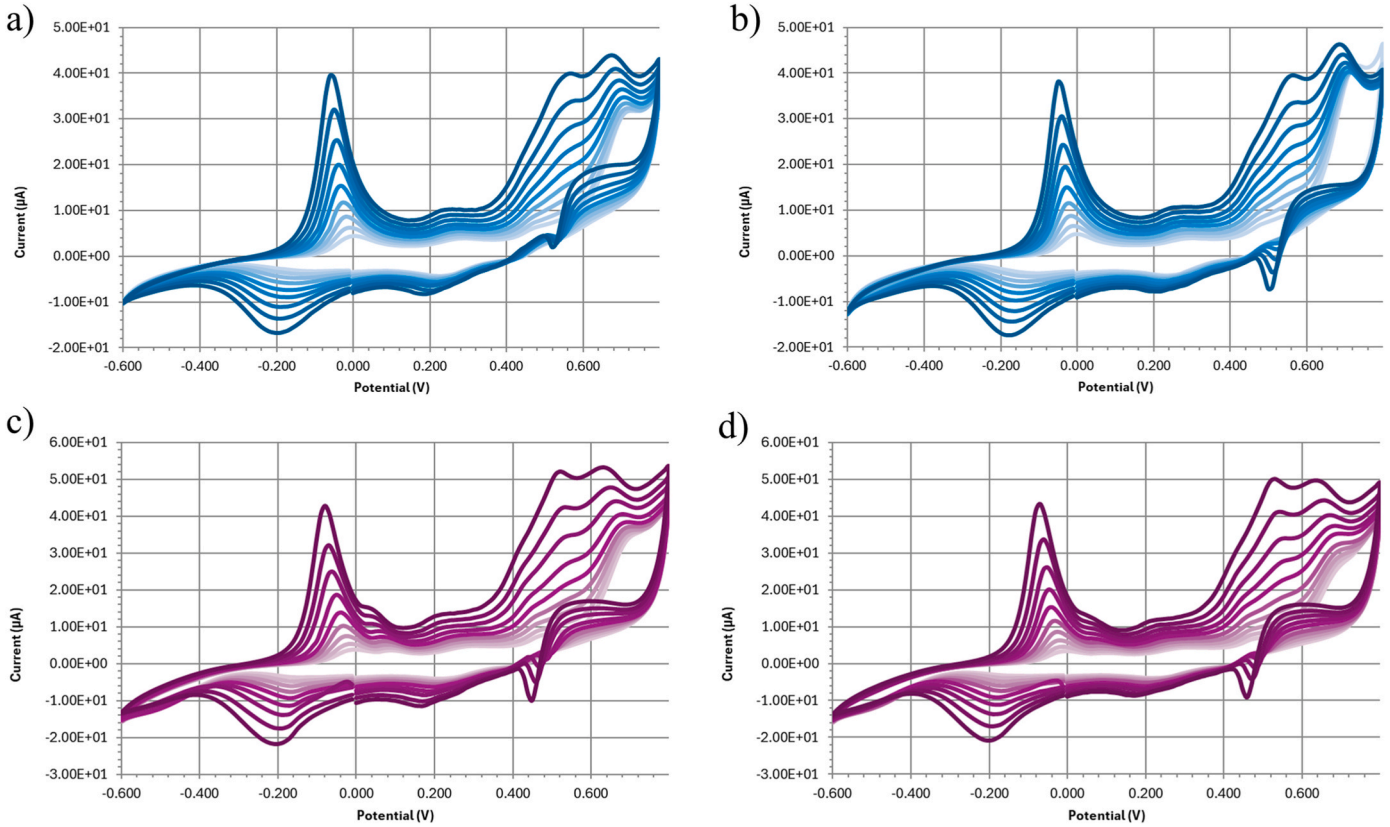

Fig. 4. Cyclic voltammetry (CV) after 15 scans of (a) BP-3 MIP, (b) BP-3 NIP, (c) OC MIP, and (d) OC NIP, in optimized conditions.

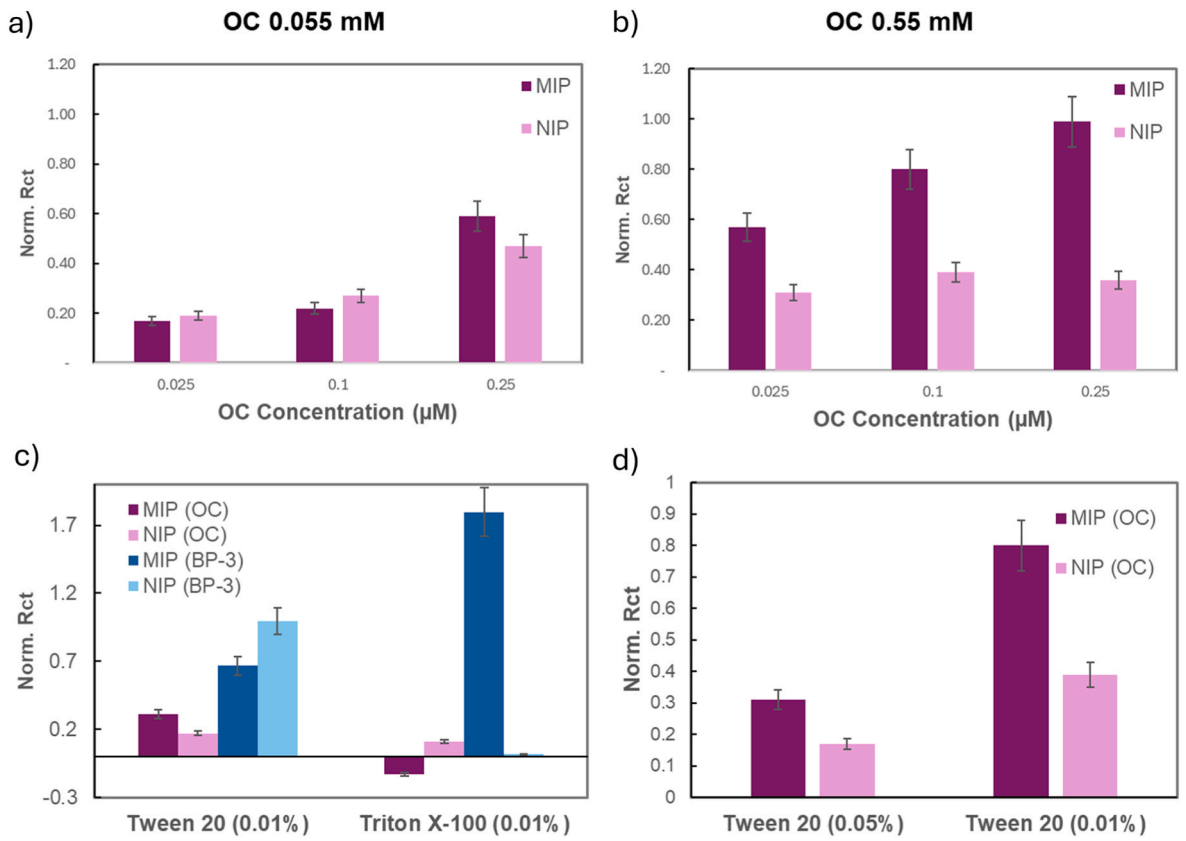

Fig. 5. Re-binding test response at three OC concentrations (0.025, 0.1, and 0.25 μM) for NIP and MIP sensors synthesized with different template concentrations: (a) 0.055 mM and (b) 0.55 mM; (c) MIPs and NIPs responses to 0.25 μM of OC and 0.5 μM of BP-3 after blocking with Tween 20 (0.01 %, v/v) and Triton X-100 (0.01 %, v/v); (d) MIP and NIP response to 0.25 μM of OC after the blocking with Tween 20 (0.01 % and 0.05 %, v/v). Standard deviations were calculated based on measurements performed in triplicate.

3.2. MIP/NIP characterization

Scanning Electron Microscope (SEM) analysis was carried out using a Supra 40 Field Emission Microscope (Carl Zeiss AG, Oberkochen, Germany) to capture secondary electron emissions at a primary beam acceleration voltage of 2.5 kV, examining the gold electrode surface both before and after the deposition of the MIP/NIP layer (Fig. 6). SEM images shown in Fig. 6a and b revealed the presence of a colored polymer layer finely deposited on the surface of the bare globular gold electrode.

Fourier Transform Infrared Spectroscopy (FTIR) spectra were recorded using a Jasco 6200 in conjunction with PIKE MIRacle ATR accessory, scanning the spectral range from 500 to 4000 cm^{-1}. The FTIR spectrum of the blocked polyaniline layer (Fig. 6c, purple line) was compared to that of the bare gold electrode (Fig. 6c, blue line), revealing characteristic IR bands associated with N–H bond vibrations (3400 cm^{-1}), whose low intensity is most likely due to the surface blocking, C–H stretching (2900 cm^{-1}), C═C (1650 cm^{-1}), C–C aromatic (1600 cm^{-1}), and C–N aromatic (1255 cm^{-1}), confirming the successful

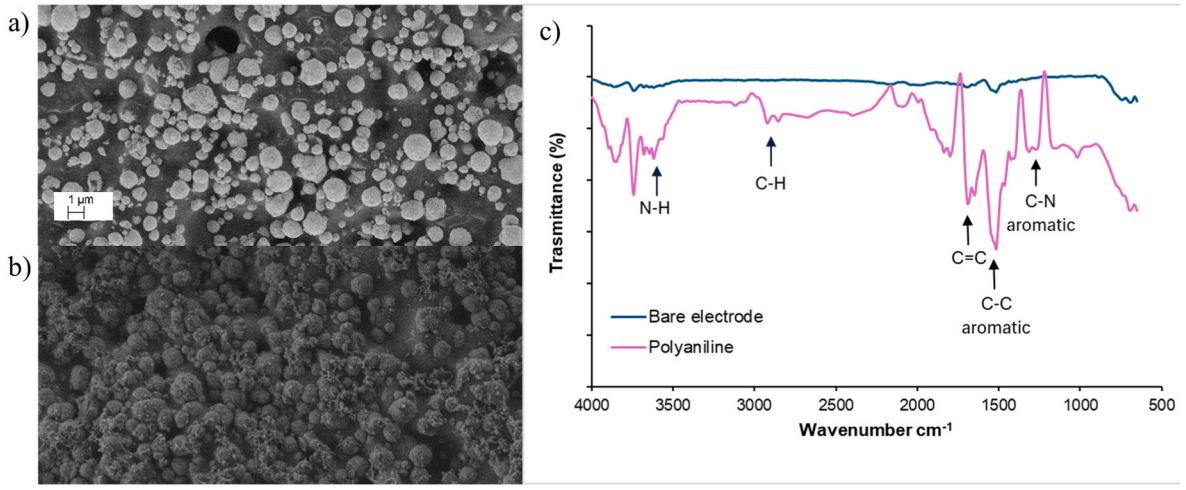

Fig. 6. Scanning Electron Microscope (SEM) of the gold bare electrode (a) and the polyaniline layer (b). Fourier Transform Infrared Spectroscopy (FTIR) spectra of the gold bare electrode and the polyaniline layer (c).

deposition of the polyaniline layer onto the SPGE.

Contact angle measurements were performed using the tensiometer ATTENSION from Biolin Scientific UK (Stockport, UK) at different stages of electrode preparation to assess changes in hydrophilic or hydrophobic properties. As shown in Fig. 7 and Table 1, the bare electrode exhibited a hydrophobic surface with a contact angle significantly higher compared to the MIP- and NIP-modified electrodes. In fact, a decrease in hydrophobicity was observed from the bare electrode to both the NIP and MIP sensors, attributed to the properties of polyaniline. The presence of hydrophobic templates such as BP-3 and OC further explains why the MIP exhibited approximately 15° higher hydrophobicity than the NIP. However, this difference disappears after the washing step, with both electrodes displaying contact angles in the range of 97–100°. This similarity suggests the effective removal of templates from the MIP cavities during washing, as the elimination of hydrophobic templates renders the surface characteristics more similar to those of the NIP. After the blocking step, a slight difference in contact angles between the MIP and NIP was observed (with a mean contact angle of 74° vs. 82°), but this variation falls within the standard deviation of the measurements, indicating comparable hydrophobicity of the two surfaces.

The fabrication process of both developed sensors demonstrated good reproducibility, as shown by the CV oxidation peaks in Fig. 8. The BP-3-MIP sensor exhibited a mean current of 36.15 ± 3.68 μA, while the OC-MIP sensor showed a mean current of 40.00 ± 5.35 μA (Table S1). These consistent current values highlight the reliable and repeatable performance of the sensors.

3.3. Sensor sensitivity

Re-binding experiments were performed under the conditions optimized for each assay. The equivalent circuit used to fit the experimental data is shown in Fig. S1. A Randles circuit was used and optimized to minimize the average fitting error associated with the Rct values resulting in a mean error of 0.99 % (±0.4 %). The Rct values were normalized as described in Section 2.5 and used to plot the calibration curves.

Figs. 9 and 10 present the calibration curves obtained using MIP and NIP electrodes for BP-3 and OC with an R^2 equal to 0.97514 and 0.95149 and slopes equal to 1.36968 and 0.31987, respectively. The MIP electrodes showed a clear correlation between the signal and the concentration of both BP-3 and OC, demonstrating the specific recognition capabilities of the imprinted polymers. In contrast, the control NIP electrodes showed minimal response, likely due to a residual degree of non-specific interactions still present between the analytes and the polyaniline layer despite the optimization of the washing and blocking procedures. The remarkable difference in response between MIP and NIP suggests that the observed signal from the MIP is primarily due to the specific binding of the target compounds to the imprinted sites.

The limit of detection (LOD) was calculated as the concentration equal to three times the standard deviation of the blank signal divided by the slope of the calibration curve, while the limit of quantification (LOQ) was calculated as the concentration equal to ten times the standard deviation of the blank signal divided by the slope of the calibration curve. Under the optimized conditions, the sensors demonstrated the ability to detect BP-3 and OC with LOD of 30 nM and 1 nM, respectively.

Table 1
Mean contact angle meter measurements and respective standard deviation of the gold bare electrode, the MIP, and the NIP at different stages of the electrode preparation procedure. Standard deviations were calculated by averaging the left and right angles of measurements performed in triplicate.

Procedure step	Bare	MIP	NIP
	Angle ± Std dev (°)	Angle ± Std dev (°)	Angle ± Std dev (°)
Polymerization	109.77 ± 0.74[a]	85.68 ± 0.42	70.45 ± 5.89
Washing		100.40 ± 0.5	96.92 ± 0.68
Blocking		73.58 ± 13.20	81.92 ± 1.99

[a] Mean contact angle value of the bare electrode before polymerization.

The linear detection range was between 40 nM and 1 μM for BP-3 and 10 nM–50 nM for OC.

3.4. Cross-reactivity

Selectivity experiments were conducted for both electrodes, the one optimized for BP-3 detection and the other for OC, in the presence of two additional potential interferents, ibuprofen and paracetamol. These pharmaceutical compounds were selected based on their chemical structure, which contains aromatic groups similar to those in the target analytes, as well as their dimensions, comparable to (or smaller) than the template molecules. These characteristics could potentially allow the interferents to penetrate and bind within the cavities of the MIP layers. Moreover, given their widespread use and frequent detection in wastewater, ibuprofen and paracetamol represent common contaminants relevant to this study.

Each analyte at a known concentration (0.1 μM) was incubated in parallel on the sensor surfaces, and EIS spectra were recorded. Selectivity was evaluated based on the Imprinting Factor (IF), as defined in Section 2.6, with results shown in Table 2. The BP-3 selective electrode demonstrated an IF of 55 for the target analyte, indicating a strong affinity and specificity for BP-3. In contrast, all potential interferents, including OC, exhibited IF values below 1, suggesting no specific affinity for these compounds and only non-specific binding to the NIP surface.

For the OC-selective sensor, the MIP showed a higher response compared to the NIP, with an IF of 2.26 for OC, while the IF values for ibuprofen and paracetamol were close to 1. Since IFs above 1 are associated with a reliable level of specificity in the affinity sensor field [19], this indicates that, unlike the target analyte, which specifically interacts with the imprinted cavities in the MIP, the interferents interact similarly with both the MIP and NIP, further confirming the sensor's specificity for OC. The relatively low IF observed for the OC-selective sensor for its target analyte, especially when compared to the IF of 55 obtained for the BP-3 selective sensor, could be explained by a limited abundance of specific binding sites. In fact, due to the low solubility of OC in the polymerization solution, a non-ideal template:monomer molar ratio of 1:45 was used in the electropolymerization step, resulting in a MIP that was probably less efficient than the one prepared for BP-3. Additional changes in the composition of the polymerization solution that would allow the amount of OC to be increased without affecting the electropolymerization of aniline (or the formation of specific cavities) could be explored in the future to further enhance the specificity of the

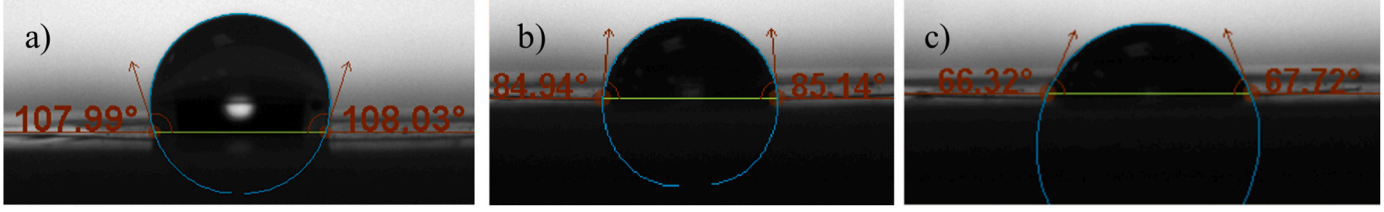

Fig. 7. Contact angle meter of the gold bare electrode (a), the MIP layer (b), and the NIP layer (c).

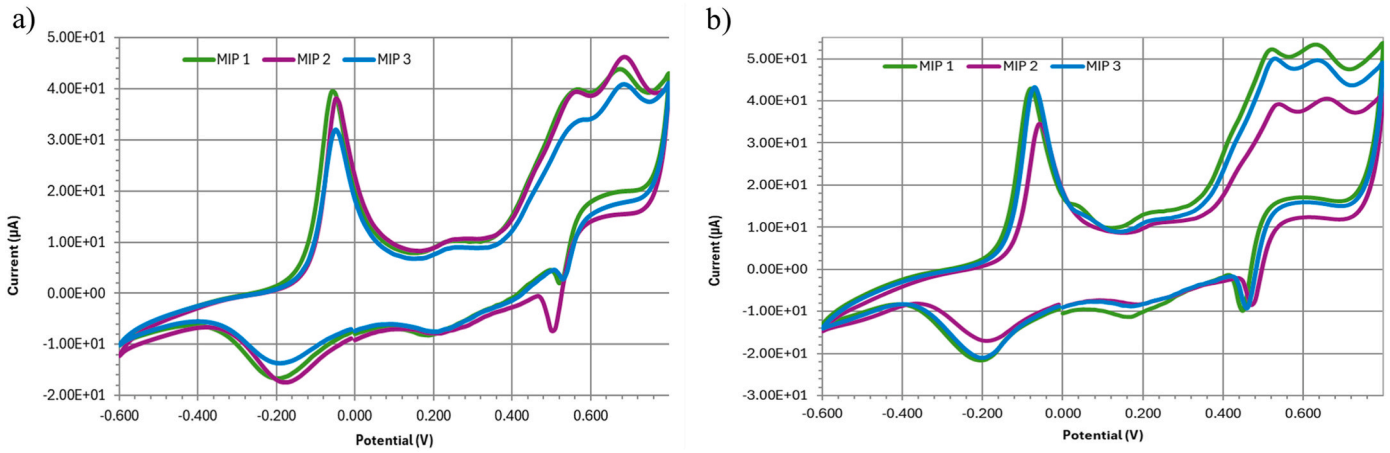

Fig. 8. Cyclic voltammetry (CV) after 15 scans of (a) three BP-3 MIPs, (b) three OC MIPs, in optimized conditions.

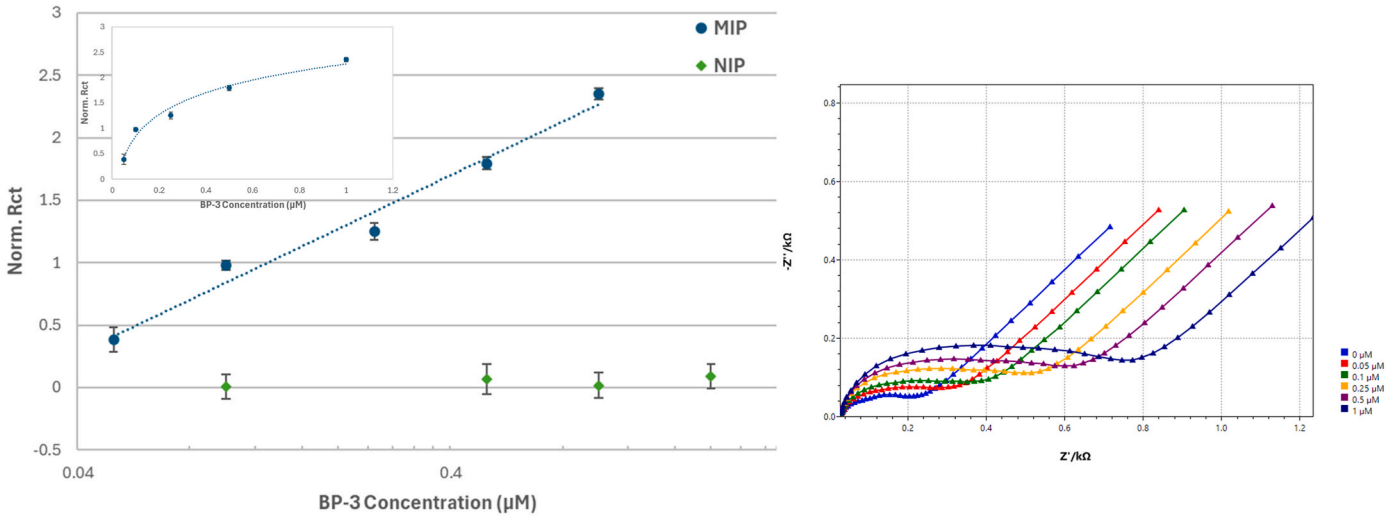

Fig. 9. Linear and nonlinear (inset) calibration (left) for MIP and NIP electrodes, and electrochemical impedance spectroscopy (EIS) curves (right) for the MIP electrode at increasing concentrations of BP-3. Standard deviations were calculated based on measurements performed in triplicate.

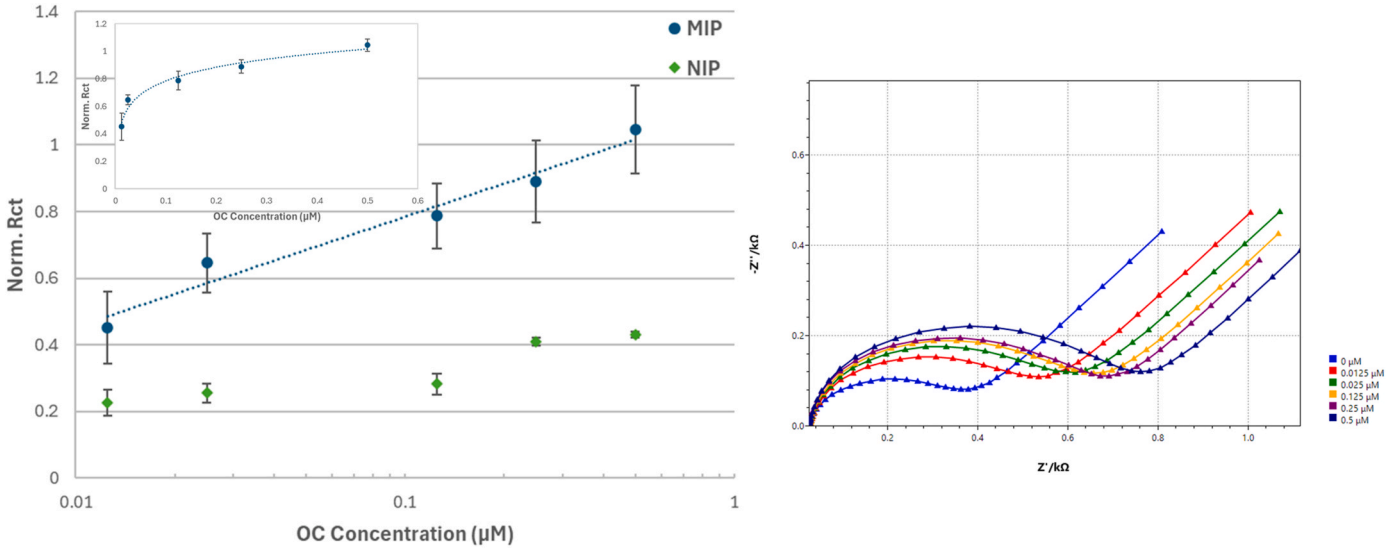

Fig. 10. Linear and nonlinear (inset) calibration curves (left) for MIP and NIP sensors and electrochemical impedance spectroscopy (EIS) curves (right) for the MIP electrodes at increasing concentrations of OC. Standard deviations were calculated based on measurements performed in triplicate.

Table 2
Selectivity results for BP-3-selective electrode (left) and OC-selective electrode (right). Expressed as an Imprinting Factor (IF).

Compound (0.1	IF	Compound (0.1 μM)	IF
Analyte (BP-3)	55	**Analyte (OC)**	2.26
OC	0.14	**BP-3**	1.52
Paracetamol	0.34	**Paracetamol**	1.18
Ibuprofen	0.68	**Ibuprofen**	1.01

OC-selective sensor. Furthermore, a high IF for BP-3 (1.52) was observed on the OC-selective sensors, especially when compared to the other interferents. This may be attributed to the similarity between OC and BP-3 consisting in the presence of two aromatic (or benzene-derivates) groups. Additionally, whereas BP-3 and OC share comparable solubility profiles, ibuprofen and paracetamol are significantly more soluble in water. Despite not being the target molecule, these factors could enable BP-3 to weakly interact with the MIP cavities designed for OC. However, this observation may pave the way for the development of sensors capable of simultaneously detecting multiple compounds belonging to the OUVA family, exploiting their structural and solubility similarities for broader detection capabilities.

3.5. Testing of wastewater samples: matrix effect and recovery

Calibration curves shown in Fig. 11 were obtained by spiking real wastewater samples with increasing concentrations of BP-3 and OC as described in section 2.7 (R^2 equal to 0.96077 and 0.94137 and slope 1.98129 and 0.43348 for BP-3 and OC, respectively). The LOD calculated for the calibrations in the real samples was 6 nM for BP-3 and 16 nM for OC. The higher LOD for OC, compared to the re-binding tests performed in buffer solutions, indicates a slight matrix effect but also suggests that there may be room for optimization of the blocking conditions for the OC-sensitive sensor. This hypothesis is supported by the buffer calibration curve of the corresponding NIP, shown in Fig. 10, which highlights residual non-specific interactions between the analyte and the polyaniline surface. Additional confirmation comes from the selectivity test summarized in Table 2, where, as explained in the previous section, the OC-selective sensor exhibited residual binding capability with BP-3 (IF 1.52). Further optimization could help minimize this cross-reactivity and improve the sensor's overall performance.

To assess the recoveries from wastewater samples using the MIP sensors, the real water samples collected from the Cranfield WWTP required spiking with known concentrations of BP-3 and OC primarily for analytical purposes, such as calculating recovery percentages and assessing matrix effects. In addition, previous chromatographic analysis had shown that BP-3 and OC levels in the outlet water of the WWTP were too low to be detected. This is consistent with the geographical location of the facility, situated in an inland region of the UK, and the type of wastewater treated, which comes solely from campus activities. Higher occurrences of organic UV filters, like BP-3 and OC, are commonly found in southern and coastal regions due to factors such as increased sunscreen use driven by the warmer climate and higher tourist numbers [20].

After spiking the samples with known concentrations of analytes prior to filtration and dilution with phosphate-citrate buffer, recoveries of 77 % ± 7 % for BP-3 and 101 % ± 14 % for OC were obtained. The high recovery for OC, close to 100 %, suggests a minimal impact of sample pretreatment, while the lower recovery for BP-3 reflects a more pronounced effect. A possible explanation for the lower recovery of BP-3 is the variability of the measurements and the partial adsorption of BP-3, either on the suspended solids removed during the filtration process or on the filter itself, which may reduce the concentration of analyte available for the detection. To address this issue, further improvements could involve testing filters made from different materials or exploring methods to avoid filtration altogether. Despite these challenges, the results are still promising, as the recoveries fall within the acceptance range of 70–120 % as outlined by the DG SANCO/2007/3131 European Quality Control Guidelines. All the performance data in terms of LOD, LOQ, and recovery % for BP-3 and OC obtained in spiked buffer solutions and spiked real WWTP effluents are summarized in Table 3.

In addition, the matrix effect was evaluated to account for potential interferences from organic matter and other compounds present in the water samples. The matrix effect in percentage (ME%) was assessed according to the following equation [21]:

$$\mathbf{ME\%} = \frac{\mathrm{Slope}_{\mathrm{matrix}}}{\mathrm{Slope}_{\mathrm{Buffer}}} \times \mathbf{100}$$

where $\mathrm{Slope}_{\mathrm{matrix}}$ is the slope of the calibration curve obtained in the

Table 3
Limit of detection (LOD) and limit of quantification (LOQ) for BP-3 and OC in spike buffer solution and real wastewater spiked samples.

Analyte	LOD (nM)	LOQ (nM)	Recovery %	Type of sample
BP-3	30	68	–	Spiked buffer
OC	1	3		
BP-3	6	8	77 %	WWTP effluent
OC	16	136	101 %	

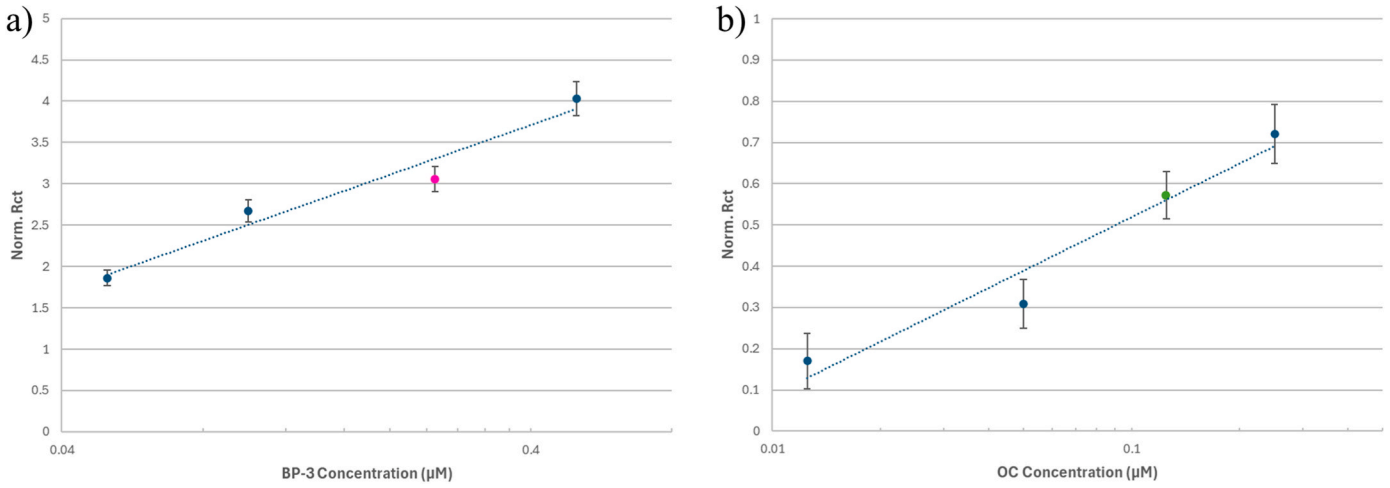

Fig. 11. Calibration curves obtained with MIP electrodes in real wastewater samples: (a) BP-3 and (b) OC. The pink and green dots represent the data points used for calculating the recovery percentages for BP-3 and OC, respectively. Standard deviations were calculated based on measurements performed in triplicate.

complex matrix samples and $Slope_{Buffer}$ is the slope of the calibration curve obtained in the buffer solution. The calculated ME% was 135 % and 144 % for OC and BP3, respectively, with 100 % representing a negligible matrix effect. Consequently, the observed effect exceeded the range of ±20 % which is commonly accepted without the need for any further optimization [22]. However, this is not uncommon with complex environmental samples such as wastewater, and a similar effect is seen even when chromatographic techniques are employed. To compensate for the medium matrix effect, several solutions can be pursued, including a dilution of the samples or the application of a Correction Factor (Cf), defined according to the following equation [23]:

$$\mathbf{C_f} = \frac{Slope_{Buffer}}{Slope_{Matrix}}$$

in this specific case, if no extra dilution is applied to the wastewater samples, a Cf of 0.69 and 0.74 for BP-3 and OC, respectively, can be applied to the calculated concentrations to account for the enhancement effect of the matrix.

The sensitivity and selectivity demonstrated with real wastewater samples combined with the straightforward synthesis, well-documented long-term durability, and stability of MIPs with a shelf-life on the order of months [24], as well as stability of polyaniline, when this is stored in a dry environment [25,26], highlight a significant potential for a reliable detection for both BP-3 and OC in complex water matrices using low-cost MIP sensors.

A direct comparison of these sensor performances with analogous devices is challenging due to the limited studies involving affinity sensors for OUVA detection. While examples of electrochemical techniques for BP-3 and OC quantification exist in literature, they typically lack a specific receptor for the target analytes. Additionally, comprehensive selectivity studies in the presence of potential interferents, critical for analyzing complex environmental samples, are often missing. Most systems are designed for different fields of application, such as the detection of BP-3 and OC in commercial cosmetic formulations [27,28]. Differently, Mutić et al. [29] developed an electrochemical method for BP-3 quantification in swimming pool water using an ionic liquid-modified carbon paste electrode and square-wave adsorptive stripping voltammetry. This device was tested against interferents commonly detected in swimming pool water samples like potassium dihydrogen phosphate (KH_2PO_4), magnesium sulfate ($MgSO_4{\cdot}7H2O$), calcium chloride ($CaCl_2$), sodium bicarbonate ($NaHCO_3$), and urea. However, wastewater samples, which are the focus of this study, present a significantly more complex matrix with a wider range of potential interferents and a high content of organic matter, highlighting the importance of a receptor specifically tailored to the selected analytes.

A comparison between the proposed MIP-based sensors and conventional chromatographic methods highlights their complementary strengths in environmental monitoring. Laboratory-based chromatographic techniques, such as HPLC and GC-MS/MS, can offer superior sensitivity but are costly, time-intensive, and unsuitable for large sample volumes or in-situ applications. These methods also lack standardized protocols, with significant variability in instrumentation and pretreatment steps, such as SPE extraction. Reported LODs for LC/GC coupled with high-resolution MS vary widely, ranging from 0.002 to 28 nM for BP-3 and 0.0008–20 nM for OC, depending on operational conditions [30–32]. In contrast, MIP sensors provide a scalable, cost-effective alternative for rapid in-situ screening of large sample volumes, which would be impractical to process using conventional methods. By identifying samples with significant analyte concentrations, the sensors enable laboratories to focus their resources on a smaller subset of samples for detailed chromatographic analysis. This integrated synergic approach enhances efficiency, reduces costs, and ensures comprehensive contaminant monitoring in complex environmental matrices.

4. Conclusions

This study represents, to the best of our knowledge, the first approach to design an affinity sensor specifically tailored for OUVA detection. Two different MIP-based electrochemical sensors were successfully developed for the quantification of BP-3 and OC, two of the most prevalent OUVAs in wastewater samples. Key optimizations, such as adjusting template concentration, pH range and surface blocking, were carried out to enhance the selectivity towards the target analytes. Contact angle, SEM, FT-IR and EIS analyses confirmed efficient polymer layer formation and effective template removal.

The proposed sensors demonstrated promising performance in complex wastewater samples, with LOD of 6 nM for BP-3 and 16 nM for OC, and recoveries of 77 % and 101 %, respectively, all within the accepted range of European guidelines. Although this study focuses on two separate MIP sensors for the individual detection of BP-3 and OC, future advancements utilizing platforms consisting of multi-channel potentiostat with SPGE with multiple working electrodes have the potential to enable the simultaneous detection of both compounds, thereby broadening the application potential of this approach.

In conclusion, the developed MIP-based sensors show strong potential for environmental monitoring, with further opportunities to improve sensor specificity and sample handling. The proposed devices present a promising solution for large-scale and in situ monitoring of OUVAs, addressing the limitations of traditional chromatographic techniques and paving the way for more comprehensive monitoring of these priority contaminants.

CRediT authorship contribution statement

Chiara Sarti: Writing – original draft, Methodology, Formal analysis, Data curation, Conceptualization. **Lea Falcon:** Formal analysis, Data curation. **Alessandra Cincinelli:** Writing – review & editing, Supervision, Resources, Project administration, Funding acquisition. **Tania Martellini:** Writing – review & editing, Supervision. **Iva Chianella:** Writing – original draft, Supervision, Project administration, Methodology, Data curation, Conceptualization.

Declaration of competing interest

The authors declare that they have no known competing financial interests or personal relationships that could have appeared to influence the work reported in this paper.

Acknowledgements

C.S. gratefully acknowledges MUR and EU-FSE for financial support of the PhD fellowship PON Research and Innovation 2014–2020 (D.M 1061/2021) XXXVII Cycle in Chemical Sciences: “Green deal and Zero Pollution strategy: innovative solutions for emerging contaminants removal”.

Appendix A. Supplementary data

Supplementary data to this article can be found online at https://doi.org/10.1016/j.talanta.2024.127375.

Data availability

Data will be made available on request.

References

[1] Y. Zhang, F. Chang, M. Junaid, H. Ju, Y. Qin, L. Yin, J. Liu, J. Zhang, X. Diao, Distribution, sources, ecological and human health risks of organic ultraviolet filters in coastal waters and beach deposits in Hainan, China, Environ. Pollut. 359 (2024) 124610, https://doi.org/10.1016/j.envpol.2024.124610.

[2] B. Kwon, K. Choi, Occurrence of major organic UV filters in aquatic environments and their endocrine disruption potentials: a mini-review, Integrated Environ. Assess. Manag. 17 (2021) 940–950, https://doi.org/10.1002/ieam.4449.
[3] N.S.R. Agawin, M.G. García-Marquez, D.R. Espada, L. Freemantle, M.G. Pintado Herrera, A. Tovar-Sanchez, Distribution and accumulation of UV filters (UVFs) and conservation status of Posidonia oceanica seagrass meadows in a prominent Mediterranean coastal tourist hub, Sci. Total Environ. 948 (2024) 174784, https://doi.org/10.1016/j.scitotenv.2024.174784.
[4] M. Carve, D. Nugegoda, G. Allinson, J. Shimeta, A systematic review and ecological risk assessment for organic ultraviolet filters in aquatic environments, Environ. Pollut. 268 (2021) 115894, https://doi.org/10.1016/j.envpol.2020.115894.
[5] C.A. Downs, E. Kramarsky-Winter, R. Segal, J. Fauth, S. Knutson, O. Bronstein, et al., Toxicopathological effects of the sunscreen UV Filter, oxybenzone (benzophenone-3), on coral planulae and cultured primary cells and its environmental contamination in Hawaii and the U.S. Virgin Islands, Arch. Environ. Contam. Toxicol. 70 (2016) 265–288.
[6] Y. Huang, J.C.F. Law, T.K. Lam, K.S.Y. Leung, Risks of organic UV filters: a review of environmental and human health concern studies, Sci. Total Environ. 755 (2021) 142486.
[7] J.F. Mao, W. Li, C.N. Ong, Y. He, M.C. Jong, K.Y. Gin, Assessment of human exposure to benzophenone-type UV filters: a review, Environ. Int. 167 (2022) 107405.
[8] S. Ramos, V. Homem, A. Alves, L. Santos, Advances in analytical methods and occurrence of organic UV-filters in the environment — a review, Sci. Total Environ. 526 (2015) 278–311, https://doi.org/10.1016/j.scitotenv.2015.04.055.
[9] P. Inaudi, M. Perrucci, F. Velocci, A. Giacomino, V. Boscaro, M. Gallicchio, E. Ugazio, O. Abollino, M. Protti, N. Lumini, M. Locatelli, R. Mandrioli, L. Mercolini, Portable voltammetry: a rapid and efficient technique for determining UV filters in cosmetics: a comparative study with HPLC-PDA and HPLC-MS/MS, Anal. Chem. 96 (34) (2024) 14004–14010, https://doi.org/10.1021/acs.analchem.4c02892.
[10] S. Campuzano, J.M. Pingarrón, Electrochemical affinity biosensors: pervasive devices with exciting alliances and horizons ahead, ACS Sens. 8 (2023) 3276, https://doi.org/10.1021/acssensors.3c01172.
[11] P. Rebelo, E. Costa-Rama, I. Seguro, J.G. Pacheco, H.P. Nouws, M.N.D. Cordeiro, C. Delerue-Matos, Molecularly imprinted polymer-based electrochemical sensors for environmental analysis, Biosens. Bioelectron. 172 (2021) 112719, https://doi.org/10.1016/j.bios.2020.112719.
[12] L. Uzun, A.P. Turner, Molecularly-imprinted polymer sensors: realising their potential, Biosens. Bioelectron. 76 (2016) 131–144, https://doi.org/10.1016/j.bios.2015.07.013.
[13] A. Chiappini, L. Pasquardini, A.M. Bossi, Molecular imprinted polymers coupled to photonic structures in biosensors: the state of art, Sensors 20 (2020) 5069, https://doi.org/10.3390/s20185069.
[14] Z. Song, M. Yin, B. Rui, T. Liu, W. Song, L. Sun, S. Li, J. Wang, M. Han, G. Gou, N. Xue, C. Liu, A novel molecularly imprinted polymer sensor for sweat cortisol with embedded probe based on the co-deposition of Prussian Blue and Polypyrrole, Sens. Actuators Rep. 8 (2024) 100217, https://doi.org/10.1016/j.snr.2024.100217.
[15] A. Korent, K.Ž. Soderžnik, S. Šturm, K.Ž. Rožman, A correlative study of polyaniline electropolymerization and its electrochromic behavior, J. Electrochem. Soc. 167 (2020) 106504, https://doi.org/10.1149/1945-7111/ab9929.
[16] W.W. Focke, G.E. Wnek, Y. Wei, Influence of oxidation state, pH, and counterion on the conductivity of polyaniline, J. Phys. Chem. 91 (1987) 5813–5818. https://pubs.acs.org/doi/10.1021/j100306a059.
[17] M.B. Regasa, T.R. Soreta, O.E. Femi, P.C. Ramamurthy, S. Kumar, Molecularly imprinted polyaniline molecular receptor-based chemical sensor for the electrochemical determination of melamine, J. Mol. Recogn. 33 (7) (2020) e2836, https://doi.org/10.1002/jmr.2836.
[18] P.U.A.I. Fernando, M.W. Glasscott, G.K. Kosgei, J.S. Cobb, E.M. Alberts, C. G. Bresnahan, T.C. Schutt, G.W. George, L.C. Moores, Toward rational design of electrogenerated molecularly imprinted polymers (eMIPs): maximizing monomer/template affinity, ACS Appl. Polym. Mater. 3 (9) (2021) 4523–4533, https://doi.org/10.1021/acsapm.1c00575.
[19] M. Mabrouk, S.F. Hammad, A.A. Abdella, F.R. Mansour, Tips and tricks for successful preparation of molecularly imprinted polymers for analytical applications: a critical review, Microchem. J. 193 (2023) 109152, https://doi.org/10.1016/j.microc.2023.109152.
[20] A. Astel, M. Stec, I. Rykowska, Occurrence and distribution of UV filters in beach sediments of the southern baltic sea coast, Water 12 (2020) 3024, https://doi.org/10.3390/w12113024.
[21] W. Zhou, S. Yang, P.G. Wang, Matrix effects and application of matrix effect factor, Bioanalysis 9 (23) (2017) 1839–1844, https://doi.org/10.4155/bio-2017-0214.
[22] H. Stahnke, S. Kittlaus, G. Kempe, L. Alder, Reduction of matrix effects in liquid chromatography–electrospray ionization–mass spectrometry by dilution of the sample extracts: how much dilution is needed? Anal. Chem. 84 (3) (2012) 1474–1482, https://doi.org/10.1021/ac202661j.
[23] Z. Chen, W.X. Huang, S. Yu, J. Yang, H. Liu, Utilization of a matrix effect to enhance the sensitivity of residual solvents in static headspace gas chromatography, J. Chromatogr. Separ. Tech. 6 (2015) 289, https://doi.org/10.4172/2157-7064.1000289.
[24] I. Chianella, A. Guerreiro, E. Moczko, J.S. Caygill, E.V. Piletska, I.M. Perez De Vargas Sansalvador, M.J. Whitcombe, S.A. Piletsky, Direct replacement of antibodies with molecularly imprinted polymer nanoparticles in ELISA—development of a novel assay for vancomycin, Anal. Chem. 85 (17) (2013) 8462–8468, https://doi.org/10.1021/ac402102j.
[25] Z. Chen, C. Wright, O. Dincel, T.-Y. Chi, J. Kameoka, A low-cost paper glucose sensor with molecularly imprinted polyaniline electrode, Sensors 20 (2020) 1098, https://doi.org/10.3390/s20041098.
[26] D. Yang, J. Wang, Y. Cao, X. Tong, T. Hua, R. Qin, Y. Shao, Polyaniline-based biological and chemical sensors: sensing mechanism, configuration design, and perspective, ACS Appl. Electron. Mater. 5 (2023) 593–611, https://doi.org/10.1021/acsaelm.2c01405.
[27] R.A. Lopes Neves, F. Moreira Araujo, F. Siqueira Pacheco, G. Chevitarese Azevedo, M.A. Costa Matos, R. Camargo Matos, Electrochemical determination of sunscreens agents in cosmetic using square wave voltammetry, Electroanalysis 31 (2019) 496, https://doi.org/10.1002/elan.201800747.
[28] A. Sunyer, A. González-Navarro, M.P. Serra-Roig, N. Serrano, M.S. Díaz-Cruz, J. M. DíazCruz, First application of carbon-based screen-printed electrodes for the voltammetric determination of the organic UV filters oxybenzone and octocrylene, Talanta 196 (2019) 381–388, https://doi.org/10.1016/j.talanta.2018.12.092.
[29] S. Mutić, J. Anojčić, M. Vraneš, J. Panić, S. Papović, Voltammetric determination of organic UV filters by carbon paste electrodes modified with pyridinium-based ionic liquids, Talanta 266 (2024) 125103, https://doi.org/10.1016/j.talanta.2023.125103.
[30] M. Ashfaq, Y. Li, Y. Wang, W. Chen, H. Wang, X. Chen, W. Wu, Z. Huang, C.P. Yu, Q. Sun, Occurrence, fate, and mass balance of different classes of pharmaceuticals and personal care products in an anaerobic-anoxic-oxic wastewater treatment plant in Xiamen, China, Water Res. 123 (2017) 655–667, https://doi.org/10.1016/j.watres.2017.07.014.
[31] K.M. Blum, P.L. Andersson, G. Renman, L. Ahrens, M. Gros, K. Wiberg, P. Haglund, Non-target screening and prioritization of potentially persistent, bioaccumulating and toxic domestic wastewater contaminants and their removal in on-site and large-scale sewage treatment plants, Sci. Total Environ. 575 (2017) 265–275, https://doi.org/10.1016/j.scitotenv.2016.09.135.
[32] A. Sunyer-Caldú, B. Benedetti, C. Valhondo, L. Martínez-Landa, J. Carrera, M. Di Carro, E. Magi, M.S. Diaz-Cruz, Using integrative samplers to estimate the removal of pharmaceuticals and personal care products in a WWTP and by soil aquifer treatment enhanced with a reactive barrier, Sci. Total Environ. 867 (2023), https://doi.org/10.1016/j.scitotenv.2023.161466.